A hybrid method for modelling damage in composites and its effect on natural frequency

B. Suliman, C.A. Featherston, D. Kennedy*

School of Engineering, Cardiff University,
Queen's Buildings, The Parade, Cardiff, CF24 3AA, United Kingdom
<SulimanBS, FeatherstonCA, KennedyD>@cardiff.ac.uk

*Corresponding author

Keywords: vibration; composite; isotropic; damage; exact stiffness; finite element

Abstract
Delamination is a frequent cause of failure in laminated structures, reducing their overall stiffness and hence their critical buckling loads. Delaminations tend to grow rapidly in postbuckling, causing further reductions in structural strength and leading ultimately to sudden structural failure. Many studies have investigated the effects of delaminations on buckling and vibration of composite structures. Finite element analysis is often used to model complex geometries, loading and boundary conditions, but incurs a high computational cost. The exact strip method provides an efficient alternative approach using an exact dynamic stiffness matrix based on a continuous distribution of stiffness and mass over the structure, so avoiding the implicit discretization to nodal points in finite element analysis. However due to its prismatic requirements, this method can model damaged plates directly only if the damaged region extends along the whole length of the plate. This paper introduces a novel combination of exact strip and finite element analysis to model more complex cases of damaged plates. Comparisons with pure finite element analysis and a previous smearing method demonstrate the capability and efficiency of this hybrid method for a range of isotropic and composite plates. The effect of damage on the lowest natural frequency is studied.

1 Introduction

Minimizing the mass of an aircraft's structure through the use of composites reduces the cost of materials and manufacturing, as well as fuel consumption and atmospheric emissions. Delamination is one of the most frequent causes of failure in composite laminate structures, particularly those subjected to compressive loads. Delaminations reduce overall compressive stiffness and can grow rapidly during postbuckling, potentially leading to sudden structural failure [1]. They can also cause significant reductions in the associated natural frequencies of the structure. Many researchers have investigated the effects of damage on the buckling or vibration behaviour of composite structures. Pekbey and Sayman [2], Lee and Park [1] and Cappello and Tumino [3] studied the interaction between local and global buckling and the location and size of a delamination. They concluded that the critical buckling load and the lowest natural frequency are decreased by increasing the delamination size or by moving the delamination depth towards the mid-thickness of the plate, with a transition from global to local mode shapes. Pre- and post-buckling behaviour of a delaminated composite laminate was examined by Karihaloo and Stang [4] who introduced guidelines for assessing the threat posed by interlaminar matrix delamination. They identified the possible source of discrepancy between the predicted and measured critical compressive stress at which the delamination buckled. Liu et al. [5] explored the postbuckling behaviour of flat composite plates with two through-the-width delaminations under compressive loading. Based on finite element results, they concluded that multiple delaminations significantly reduce the global buckling and collapse loads while the initial delamination length has little effect on the global buckling. Nikrad et al. [6] introduced a layerwise theory to investigate the postbuckling behaviour and delamination growth of geometrically imperfect composite plates. Different boundary conditions including through-the-width and edge delaminations and locations were considered. This research elaborated points that designers need to carefully consider during the computational simulation stage. Yazdani et al. [7] presented a first-order shear deformation theory, based on the finite element method, for modelling multi-layered composite laminates. This method was used to investigate the effect of delaminations in laminates with curvilinear fibres. The study revealed that the theory is effective when analysing variable stiffness composite laminates. Szekrényes [8] studied the displacement and stress fields in symmetrically delaminated, layered composite plates subjected to bending using third-order shear deformation plate theory. The study showed better results than those obtained by second-order shear deformation theory. However, differences were found when analysing normal and transverse shear stresses.

In recent years, the majority of the research carried out in this field has used finite element analysis (FEA) to model laminates incorporating one or more damaged regions[3, 7, 9-13]. FEA provides a versatile approach, capable of handling complex geometries and many combinations of load and boundary conditions for a range of damage shapes. However, even with today's computer hardware, this type of analysis still often comes at a high computational cost. During an aircraft's preliminary design stage when many alternative configurations and load cases need to be considered, fast and reliable analysis tools are required. The exact strip method [14] provides an efficient alternative approach using an exact dynamic stiffness matrix based on a continuous distribution of stiffness and mass over the structure, so avoiding the discretization to nodal points that is implicit in FEA. However due to its requirement for the geometry of the structure to be prismatic, the exact strip method can model damaged plates directly only if the damaged region extends along the whole length of the plate. Butler et al. [15] extended the method to study thin film buckling of a thin sublaminate caused by near surface delamination. Although the present paper focuses on illustrations in vibration, with a view to future identification of damage via non-destructive measurements of changes in natural frequencies, its methodology can be readily applied to the related eigenproblems of critical buckling.

The aim of this study is to introduce a novel hybrid approach which can be used to improve the ability of the exact strip method to model more complex cases of damaged plates. This approach comprises a combination of the exact strip method and finite element theory, denoted VFM (VICON [16] and Finite element Method). An outline of the exact strip method is given in section 2 below. Section 3 introduces the hybrid approach in which the undamaged part of the structure is modelled using the exact strip method, therefore taking advantage of its efficiencies, while the damaged area is modelled using FEA, allowing the more complex geometry in this area to be represented, whilst minimising the additional degrees of freedom which need to be introduced and hence the computational cost. In section 4, damaged isotropic and composite plates are studied for different sized delaminations at different locations in plane and through the thickness. For validation purposes and to demonstrate the efficiency of this technique, a comparison is made with both pure FEA and a smearing technique based on the exact strip method previously presented by Damghani et al. [17]. The solution time predictions in section 5 demonstrate the computational efficiency of the proposed method.

2 Exact strip method

Damghani et al. [18] studied the critical buckling of composite rectangular plates with through-the-length delaminations using exact stiffness analysis and an iterative search known as the Wittrick–Williams algorithm [19]. The simplest form of the exact theory assumes sinusoidal buckling or vibration mode shapes in the longitudinal direction, with all three components of the displacement varying sinusoidally along any longitudinal line with a half-wavelength λ which divides exactly into the plate length l. This is illustrated in Figure 1 which shows the perturbation edge displacements and nodal lines of a plate during buckling or vibration. Edge displacements are multiplied by $\exp(i\pi x/\lambda) * \cos(2\pi nt)$, where n is the frequency and t is time. This is the approach adopted in the computer program VIPASA [20] .

In cases where in-plane shear loading is present and the mode is skewed, however, the desired support conditions will not be satisfied, limiting the applicability of the VIPASA analysis. In these instances a VICON (VIpasa with CONstraints) analysis is utilized [16]. The key difference between VICON and VIPASA analysis is that VICON introduces Lagrangian multipliers to couple sinusoidal responses with different values of half-wavelength λ, yielding a series solution which satisfies constraints such as simply supported end conditions [21]. It is noted that the VICON analysis models an infinitely long structure whose end supports repeat at intervals of l, mimicking typical aerospace wing and fuselage panels. The VICON stiffness matrix comprises a series of VIPASA stiffness matrices and assumes that the deflections of an infinitely long plate assembly can be expressed as a Fourier series

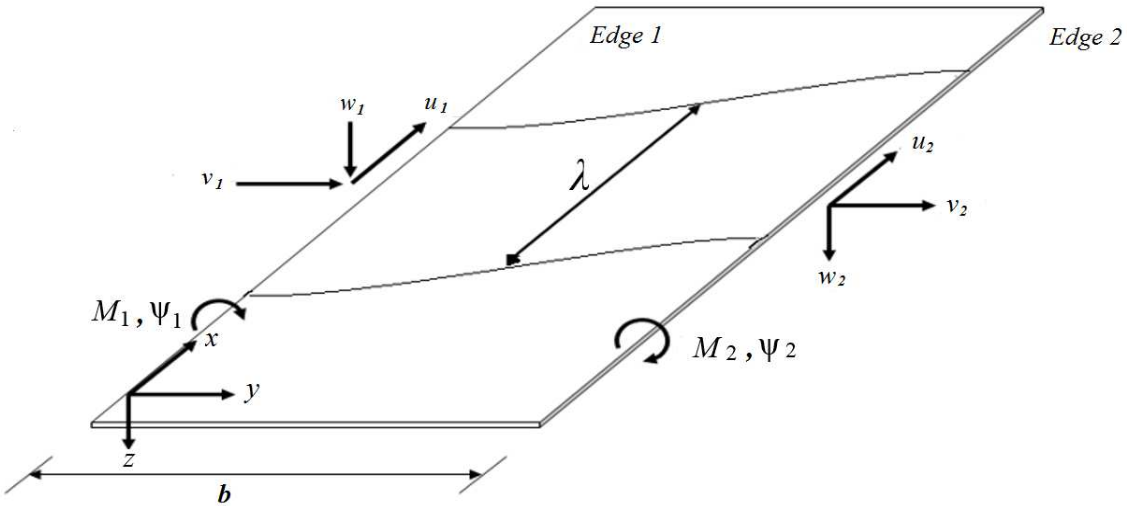

Figure 1. Rectangular plate, showing perturbation edge displacements and nodal lines

$$\boldsymbol{D}_a = \sum_{m=-\infty}^{\infty} \boldsymbol{D}_m exp(i\pi x/\lambda_m) \tag{1}$$

where $\mathbf{D}_a$ is the nodal displacement amplitude vector of the plate assembly, $\mathbf{D}_m$ are the displacement amplitude vectors from a series of VIPASA analyses,

$$\lambda_m = \frac{l}{\xi + 2m}, (0 \leq \xi \leq 1;\ m = 0, \pm 1, \pm 2, \dots, \pm q) \tag{2}$$

and the plate structure is assumed to have a mode shape that repeats at intervals of $L = 2l/\xi$. The perturbation force vectors $\mathbf{P}_a$ are similarly defined as

$$\boldsymbol{P}_a = \sum_{m=-\infty}^{\infty} \boldsymbol{K}_m \boldsymbol{D}_m exp(i\pi x/\lambda_m) \tag{3}$$

where $\mathbf{K}_m$ is the VIPASA stiffness matrix for $\lambda = \lambda_m$. The VICON stiffness equations relating $\mathbf{K}_m$, $\mathbf{D}_m$, $\mathbf{P}_m$ and the Lagrangian multipliers $\mathbf{P}_L$ are thus expressed as

$$\begin{bmatrix} l\boldsymbol{K}_0 & \boldsymbol{0} & \boldsymbol{0} & \boldsymbol{0} & \boldsymbol{0} & \dots & \boldsymbol{0} & \boldsymbol{E}_0^H \\ \boldsymbol{0} & l\boldsymbol{K}_1 & \boldsymbol{0} & \boldsymbol{0} & \boldsymbol{0} & \dots & \boldsymbol{0} & \boldsymbol{E}_1^H \\ \boldsymbol{0} & \boldsymbol{0} & l\boldsymbol{K}_{-1} & \boldsymbol{0} & \boldsymbol{0} & \dots & \boldsymbol{0} & \boldsymbol{E}_{-1}^H \\ \boldsymbol{0} & \boldsymbol{0} & \boldsymbol{0} & l\boldsymbol{K}_2 & \boldsymbol{0} & \dots & \boldsymbol{0} & \boldsymbol{E}_2^H \\ \boldsymbol{0} & \boldsymbol{0} & \boldsymbol{0} & \boldsymbol{0} & l\boldsymbol{K}_{-2} & \dots & \boldsymbol{0} & \boldsymbol{E}_{-2}^H \\ \vdots & \vdots & \vdots & \vdots & \vdots & \ddots & \vdots & \vdots \\ \boldsymbol{0} & \boldsymbol{0} & \boldsymbol{0} & \boldsymbol{0} & \boldsymbol{0} & \dots & l\boldsymbol{K}_{-q} & \boldsymbol{E}_{-q}^H \\ \boldsymbol{E}_0 & \boldsymbol{E}_1 & \boldsymbol{E}_{-1} & \boldsymbol{E}_2 & \boldsymbol{E}_{-2} & \dots & \boldsymbol{E}_{-q} & \boldsymbol{0} \end{bmatrix} \times \begin{bmatrix} \boldsymbol{D}_0 \\ \boldsymbol{D}_1 \\ \boldsymbol{D}_{-1} \\ \boldsymbol{D}_2 \\ \boldsymbol{D}_{-2} \\ \vdots \\ \boldsymbol{D}_M \\ \boldsymbol{P}_L \end{bmatrix} = \begin{bmatrix} \boldsymbol{P}_0 \\ \boldsymbol{P}_1 \\ \boldsymbol{P}_{-1} \\ \boldsymbol{P}_2 \\ \boldsymbol{P}_{-2} \\ \vdots \\ \boldsymbol{P}_M \\ \boldsymbol{0} \end{bmatrix} \tag{4}$$

where a superscript H denotes the Hermitian transpose. $\mathbf{E}_m$ are the constraint matrices for the bay $0 \leq x < l$ and contain terms of the form $\exp(i\pi x/\lambda_m)$. Details of their derivation are given by Anderson et al. [16].

The stiffness matrix in Eq. (4) may be partitioned as

$$\boldsymbol{K}_{VICON} = \left[\begin{array}{c:c} \boldsymbol{K}_{Global\,VIPASA} & \boldsymbol{C}^{H} \\ \hdashline \boldsymbol{C} & \boldsymbol{0} \end{array}\right] \tag{5}$$

where

$$\boldsymbol{K}_{Global\,VIPASA} = \begin{bmatrix} l\boldsymbol{K}_0 & \boldsymbol{0} & \boldsymbol{0} & \boldsymbol{0} & \boldsymbol{0} & \dots & \boldsymbol{0} \\ \boldsymbol{0} & l\boldsymbol{K}_1 & \boldsymbol{0} & \boldsymbol{0} & \boldsymbol{0} & \dots & \boldsymbol{0} \\ \boldsymbol{0} & \boldsymbol{0} & l\boldsymbol{K}_{-1} & \boldsymbol{0} & \boldsymbol{0} & \dots & \boldsymbol{0} \\ \boldsymbol{0} & \boldsymbol{0} & \boldsymbol{0} & l\boldsymbol{K}_2 & \boldsymbol{0} & \dots & \boldsymbol{0} \\ \boldsymbol{0} & \boldsymbol{0} & \boldsymbol{0} & \boldsymbol{0} & l\boldsymbol{K}_{-2} & \dots & \boldsymbol{0} \\ \vdots & \vdots & \vdots & \vdots & \vdots & \ddots & \boldsymbol{0} \\ \boldsymbol{0} & \boldsymbol{0} & \boldsymbol{0} & \boldsymbol{0} & \boldsymbol{0} & \dots & l\boldsymbol{K}_{-q} \end{bmatrix} \tag{6}$$

and

$$\boldsymbol{C} = [\boldsymbol{E}_0 \quad \boldsymbol{E}_1 \quad \boldsymbol{E}_{-1} \quad \boldsymbol{E}_2 \quad \boldsymbol{E}_{-2} \quad \cdots \quad \boldsymbol{E}_{-q}] \tag{7}$$

Because the VIPASA stiffness matrices (unlike their FEA counterparts) account exactly for the effects of member loads and vibration, $\mathbf{K}_{VICON}$ is a transcendental function of load factor or frequency, and its eigenvalues (i.e. critical buckling loads or natural frequencies) are found iteratively using the Wittrick-Williams algorithm [19].

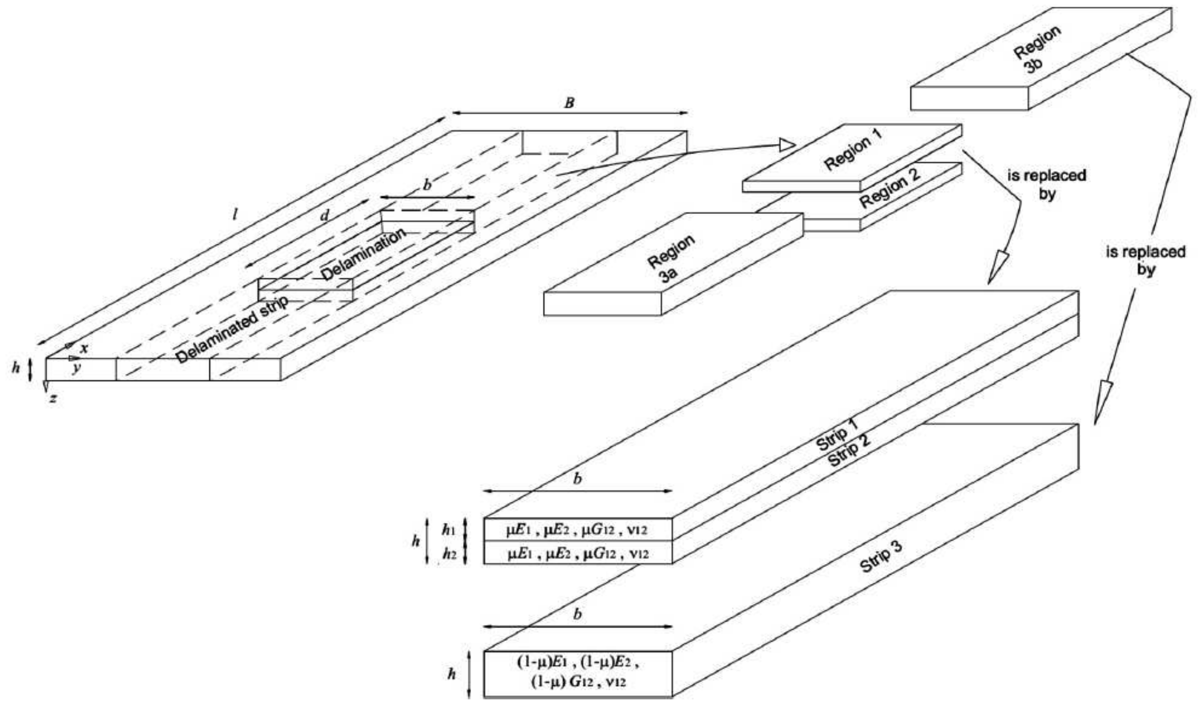

Figure 2. Smeared model for a laminate of length l, width B and thickness h, having an embedded rectangular delamination of length $d = \mu l$ and width b, reproduced from [17].

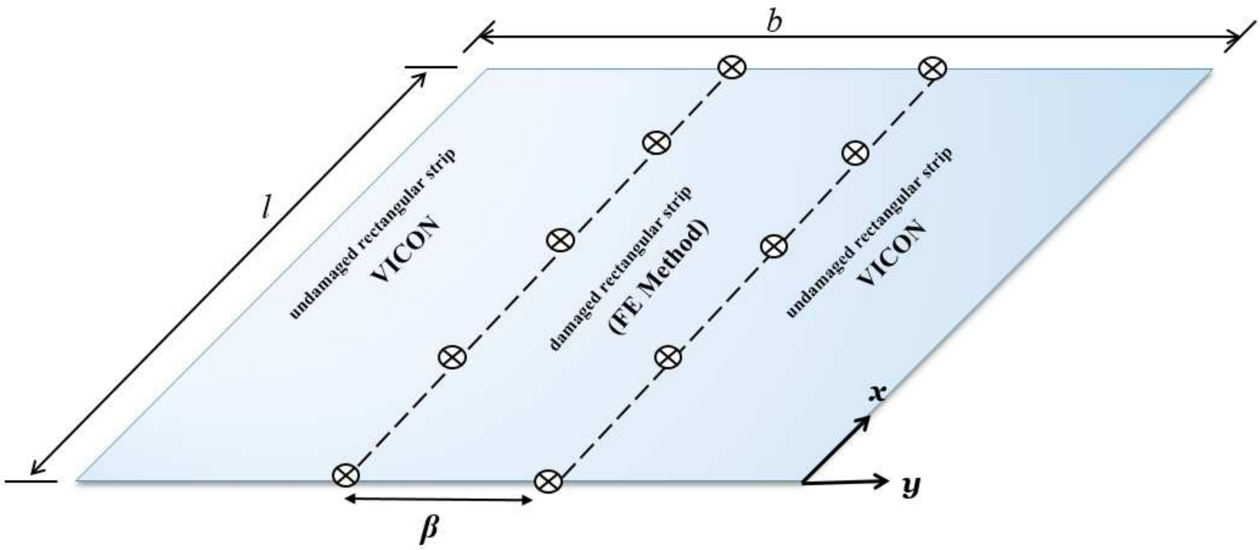

Figure 3. Damaged plate modelled by VICON and FEA (VFM).

This approach was extended by Damghani et al. [17] to cover non-prismatic scenarios including composite plates with embedded rectangular delaminations through the introduction of a smearing method (SM) in which the non-prismatic portion of the structure is replaced by an equivalent prismatic portion whose component strips have equal length l as shown in Figure 2.

3 The hybrid method VFM

In this paper, a novel combination of VICON and FEA is used to more accurately model isotropic and composite plates with either through-the-length damage or embedded damage which causes reduced stiffness in a localised area, for instance due to delaminations or matrix cracking. The proposed approach, denoted VFM (VICON and Finite element Method), uses FEA to model the longitudinal portion of the plate containing the damage as shown in Figure 3, and VICON analysis to more efficiently model the remainder of the plate. Thus VICON is used to calculate the dynamic stiffness matrices for the undamaged regions, while the FE method is used to calculate the static stiffness and mass matrices for the damaged rectangular strip. Embedded damage is modelled by including elements with different stiffness properties within this strip. Delamination within the plane of the plate is modelled by creating separate elements for the portions above and below the delamination region, with thicknesses dependent on the depth of the delamination.

ABAQUS/Standard [22] was used in all cases to validate the results obtained from VFM. Models were constructed using a four noded shell element with reduced integration and using five degrees of freedom per node (S4R5) homogeneous continuum shell elements. A rectangular mesh was used with the same number and size of elements to model the strip containing the centrally located rectangular delamination as was used for the VFM model, in order to achieve the maximum possible equivalence between the two. The element size was specified based on the results of a convergence study to determine the minimum mesh density needed for accurate results.

Figure 4 (a) shows how VFM is used to model a plate with a centrally located embedded rectangular delamination. The nodes marked with circles (●) at the boundaries between the VICON and FE regions, and at the boundary of the delamination, are treated as master nodes. Those at the same locations and marked with stars (*) are treated as slave node whose displacements and rotations are constrained to match those of the master nodes. The blue line shows the regions where boundary conditions are applied. Each node in the strips modelled using exact strip method (●) or the FE equations ($*$) is assumed to have the degrees of freedom of vertical displacement w, rotation about the x-axis θ_x and rotation about the y-axis θ_y. At the constraint locations w and θ_x are forced to be equal at the shared nodes. However, it was found that coupling θ_y made no difference to the results. Figure 4 (b) is an example of the way ABAQUS is used to model a plate to include the same number and size of elements that VFM used to model the strip containing a centrally located rectangular delamination. In both methods the displacements at the edges of the plates are constrained to apply simply supported boundary condition of the plates, i.e. in-plane displacements on the x and y axes and vertical out-of-plane displacement. The Wittrick-Williams algorithm is used to find the critical buckling loads and natural frequencies for the damaged plate.

The hybrid global dynamic stiffness matrix of the plate is formed by using Lagrangian multipliers to couple the VICON and FEA components, as follows:

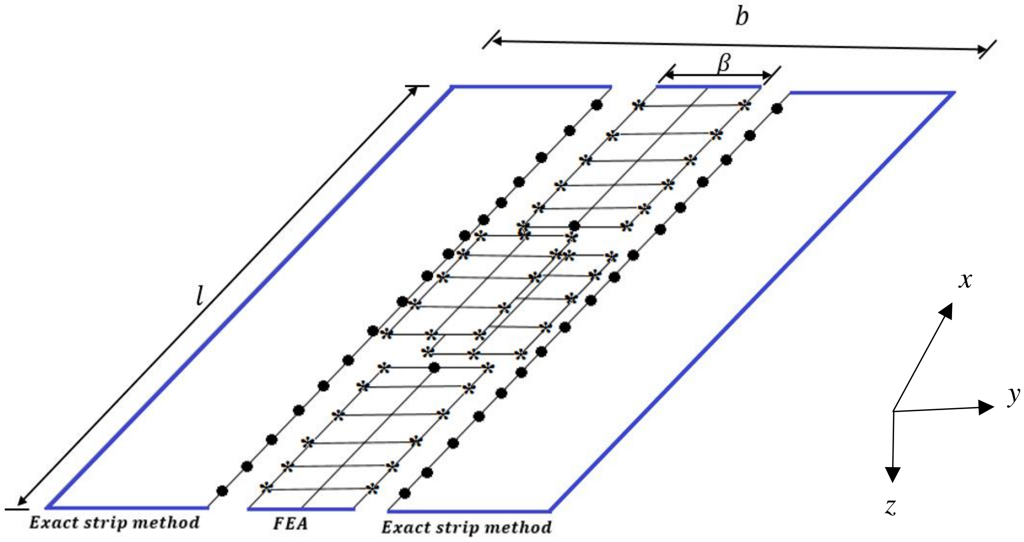

(a)

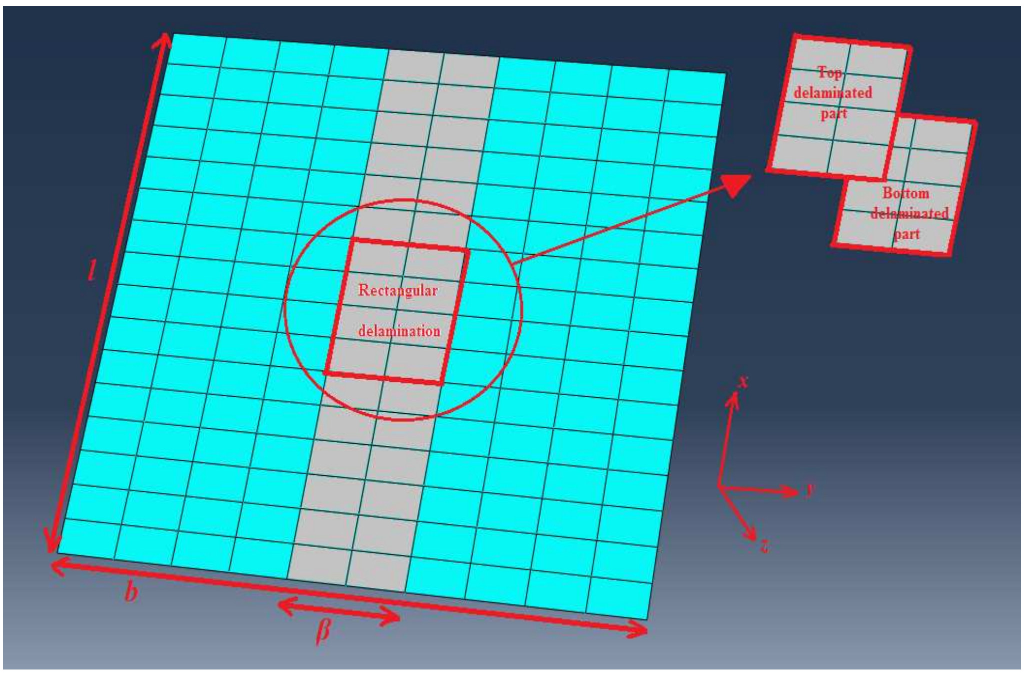

(b)

Figure 4. Identical plates containing embedded delaminations modelled by (a) VFM (b) ABAQUS.

$$
\boldsymbol{K}_{Global} = \begin{bmatrix} \boldsymbol{K}_{\ Global\,VIPASA} & \boldsymbol{0} & \boldsymbol{C}_1{}^H \\ \boldsymbol{0} & \boldsymbol{K}_{FE} & \boldsymbol{C}_2{}^T \\ \boldsymbol{C}_1 & \boldsymbol{C}_2 & \boldsymbol{0} \end{bmatrix} \tag{8}
$$

Here the constraint matrix $\mathbf{C}_1$ includes coefficients from the series solution illustrated in Eq. (1), while $\mathbf{C}_2$ includes coefficients of -1, to equate the displacements and rotations at the master and slave nodes. $\mathbf{C}_1$ also includes any support conditions in the undamaged regions. $\mathbf{C}_2{}^T$ is the transpose of $\mathbf{C}_2$ and $\mathbf{K}_{FE}$ is the FEA dynamic stiffness matrix for the damaged rectangular strip and takes the form

$$
\boldsymbol{K}_{FE} = \boldsymbol{k} - n^2\boldsymbol{m} \tag{9}
$$

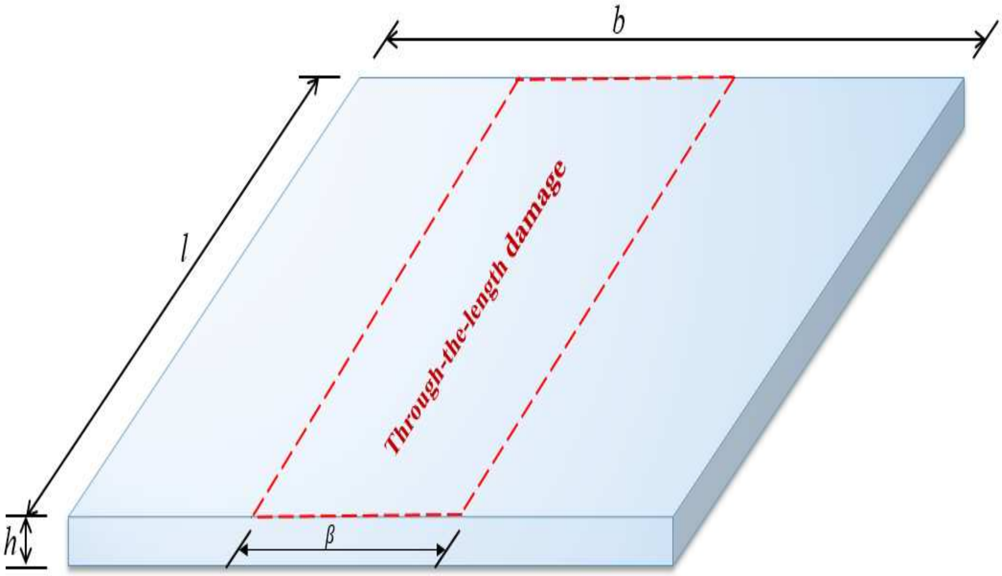

(a)

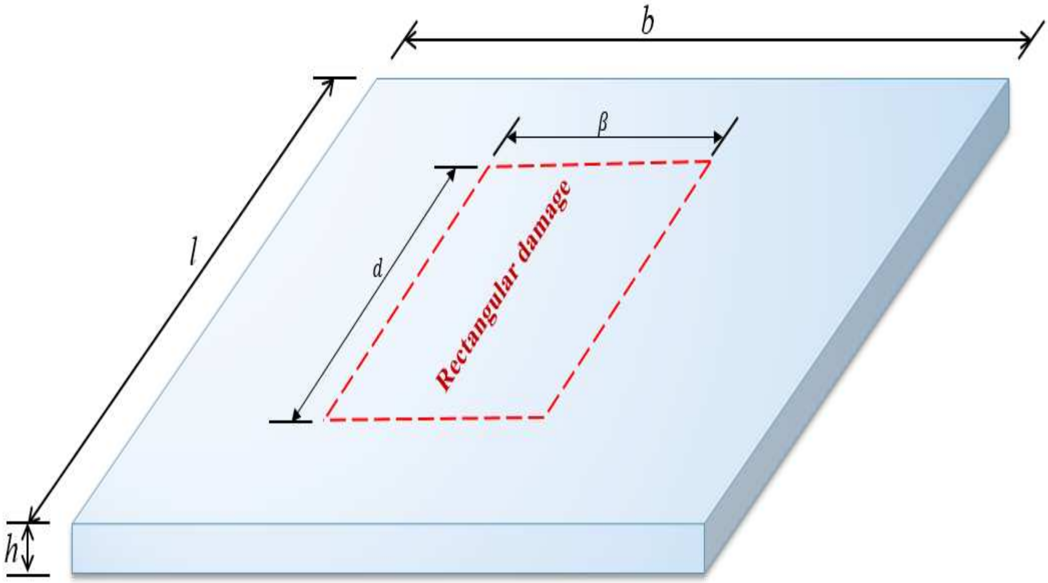

(b)

Figure 5. Plate containing centrally located (a) through-the-length damage, (b) embedded rectangular damage.

where n is the frequency and $\mathbf{k}$ and $\mathbf{m}$ are the static stiffness matrix and equivalent mass matrix of the damaged rectangular strip. Four noded rectangular elements are used with three degrees of freedom at each node, namely out-of-plane displacement and rotation about the x and y axes. The equations used for the calculation of $\mathbf{k}$ and $\mathbf{m}$ are detailed by Przemieniecki [23].

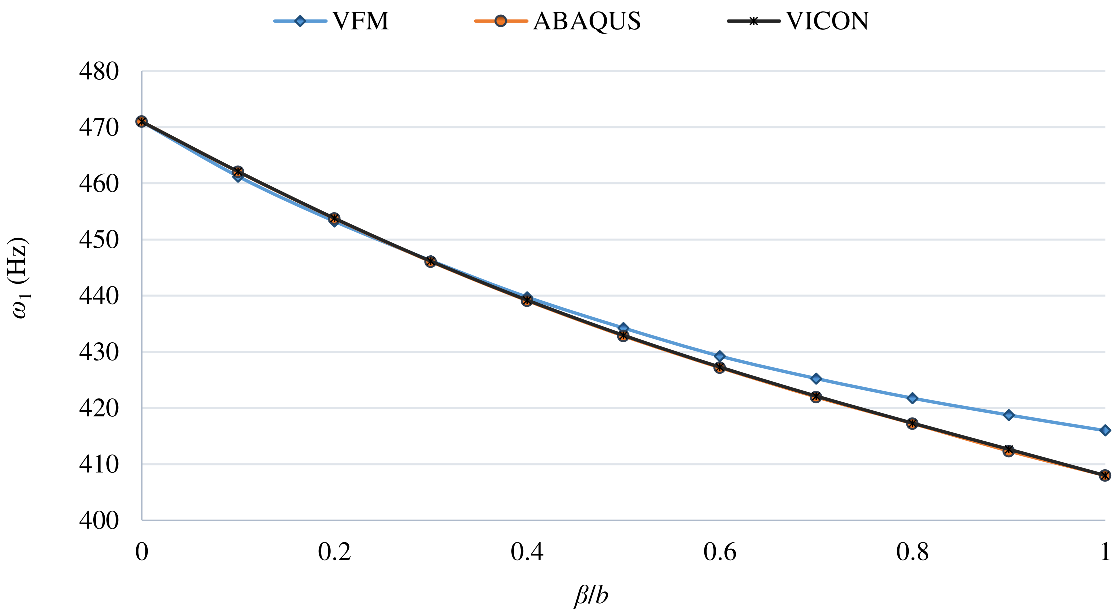

(a)

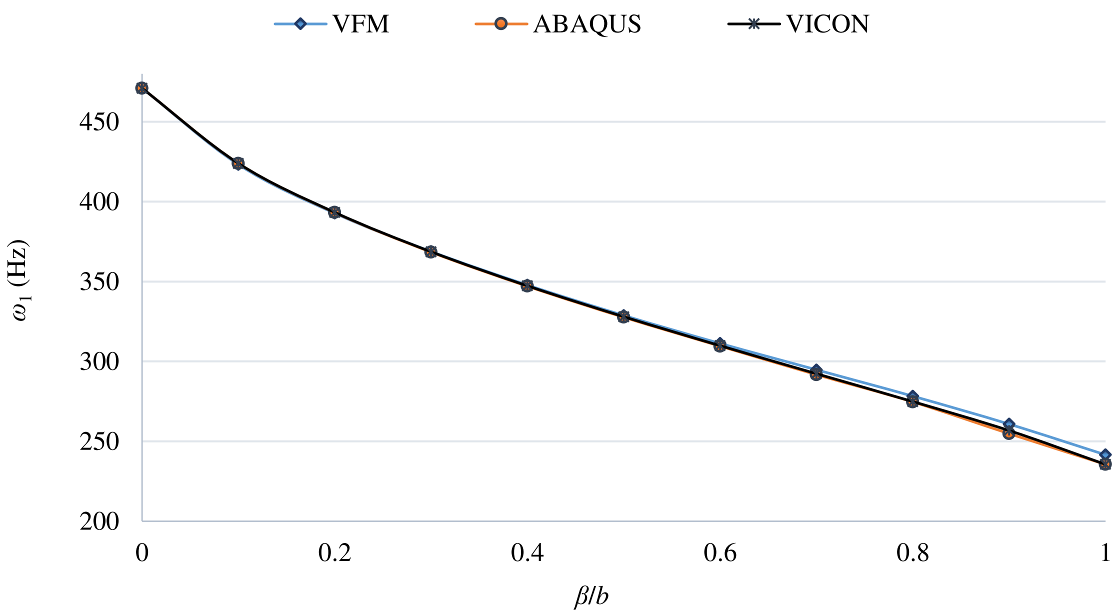

(b)

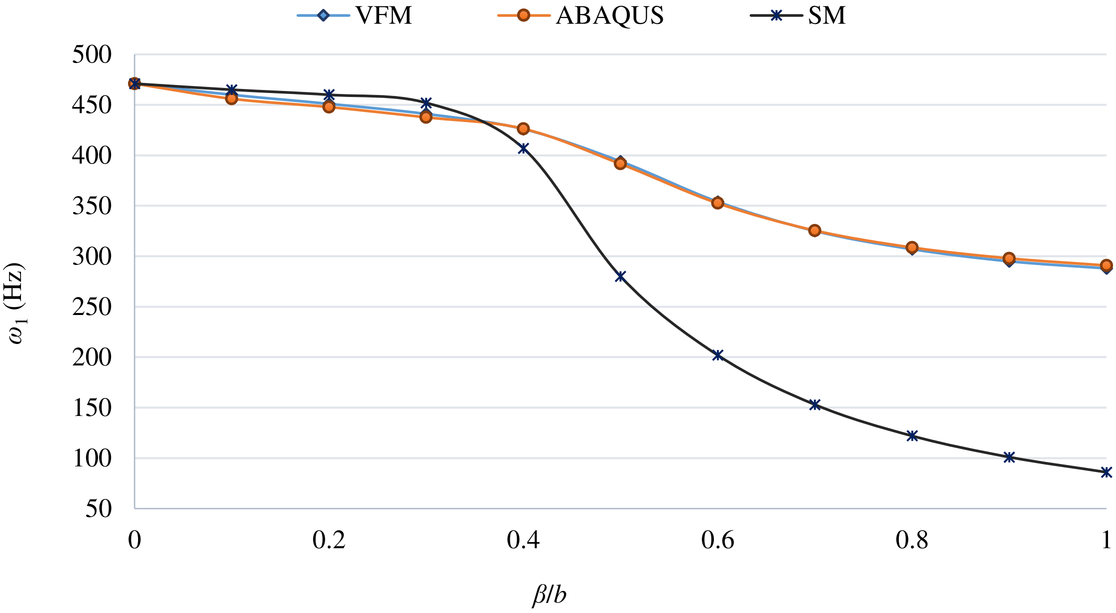

(c)

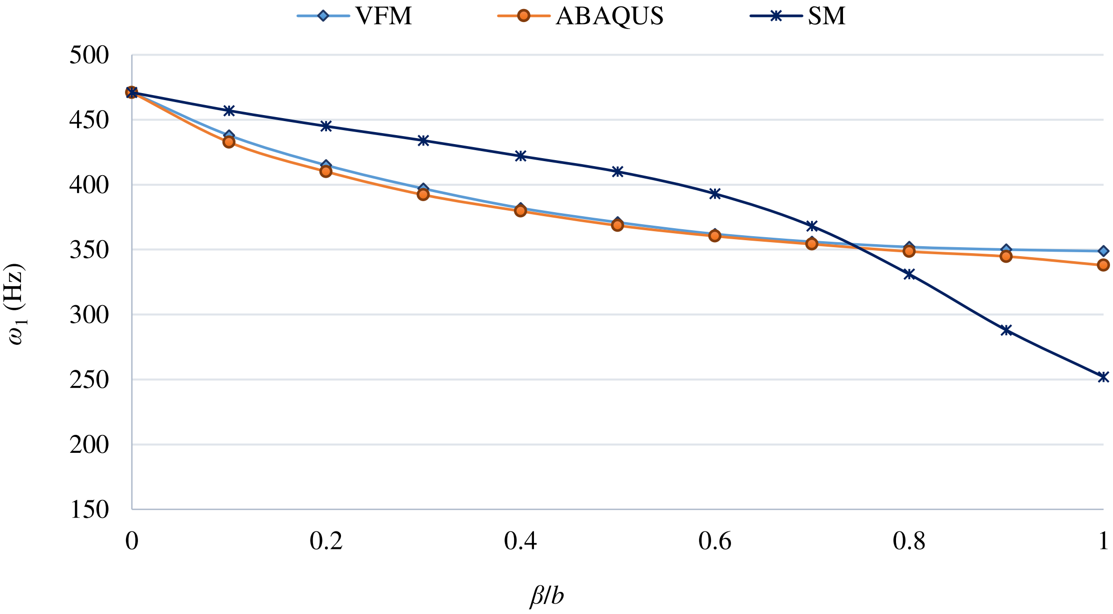

(d)

Figure 6. Plots of lowest natural frequency (ω_1) of isotropic plates against width ratio (β/b) for centrally located damage using VFM, ABAQUS and VICON or SM. (a) Through-the-length damage $(d = l)$ and $f = 0.75$. (b) Through-the-length damage $(d = l)$ and $f = 0.25$. (c) Embedded rectangular damage, $(d = 0.5l)$ and $f = 0.67$. (d) Embedded rectangular damage, $(d = 0.5l)$ and $f = 0.3$.

4 Numerical results

In order to validate the proposed model, the natural frequencies of a range of simply supported isotropic and composite plates containing through-the-length and embedded damage have been determined using VFM, SM, VICON analysis and the FEA software ABAQUS [22]. The damage modelled includes areas of reduced stiffness and delaminations. However, contact modelling is ignored in this work but will be considered in future work to enhance the accuracy of the proposed technique. Figure 5 illustrates cases of plates containing centrally located through the length and embedded damage. For simplicity, a rectangular damage shape is assumed to illustrate the hybrid method. Circular and elliptical regions of damage could be modelled by refining the mesh in the FEA strip.

4.1 Reduced stiffness isotropic plates

Figure 6 details the results of analyses for isotropic plates having length $l = 100$ mm, width $b = 100$ mm and thickness $h = 1$ mm with material properties Young's modulus $E = 110\ \text{kNmm}^{-2}$, density $\rho = 2.3 \times 10^{-6}\ \text{kgmm}^{-3}$ and Poisson's ratio $\nu = 0.3$. Damage is assumed to occur over a centrally located rectangular region of length $d\ (0 \leq d \leq l)$ and width $\beta\ (0 \leq \beta \leq b)$, and is represented generically by a stiffness reduction factor $f\ (0 \leq f \leq 1)$. VFM, ABAQUS and VICON were used to find the lowest natural frequencies of isotropic plates with through-the-length damage $(d = l)$. Figures 6 (a) and (b) show a perfect match is achieved between VICON and ABAQUS for all widths of through-the-length damage. For $0 \leq \beta \leq 0.4b$, VFM is also seen to match these results. However, as the damage width increases, i.e. for $\beta > 0.4b$, VFM predicts higher natural frequencies than both VICON and ABAQUS albeit with a maximum difference of only 1.55% at $\beta = b$. This is believed to be due to the increasing element size used in the finite element part of the VFM model. Figures 6 (c) and (d) present the first natural frequencies of isotropic plates containing embedded rectangular damage of length $d = 0.5l$ with different severities f, as calculated using VFM, ABAQUS and SM. Excellent agreement is demonstrated between VFM and ABAQUS in modelling the embedded damage. In SM the embedded rectangular damage is modelled indirectly, see Figure 2. This leads to very good agreement with the other methods when the plate vibrates globally $(0 \leq \beta \leq 0.3b)$, but when the plate vibrates locally $(\beta > 0.3b)$ SM predicts a fictitious conservative local behaviour.

4.2 Delaminated composite plates

Figure 7 compares the lowest natural frequencies for a delaminated composite plate of length $l = 100$ mm, width $b = 100$ mm and thickness $h = 4$ mm and material properties Young's moduli $E_1 = 110\ \text{kNmm}^{-2}$, $E_2 = 10\ \text{kNmm}^{-2}$, shear moduli $G_{12} = G_{13} = G_{23} = 5\ \text{kNmm}^{-2}$, major Poisson's ratio $\nu_{12} = 0.33$ and density $\rho = 4480 \times 10^{-6}\ \text{kgmm}^{-3}$. The composite comprises 32 unidirectional plies of thickness 0.125 mm in the sequence $[0/45/\text{-}45/90/90/\text{-}45/45/0/0/45/\text{-}45/90/90/\text{-}45/45/0]_S$. Embedded delaminations of width $\beta\ (0 \leq \beta \leq b)$ and two different lengths ($d = 0.25l$ and $d = 0.5l$) are added at two different depths ($0.25h$ and $0.5h$) below the top surface. The plates are analysed using VFM, ABAQUS and SM.

Figures 7 (a) and (b), in which the delamination length $d = 0.25l$ show very good agreement between VFM and ABAQUS with maximum differences of 1.88% and 3.4% for delamination depths $0.25h$ and $0.5h$, respectively, occurring when $\beta = b$. In Figures 7 (c) and (d), where the delamination length $d = 0.5l$, the maximum difference is less than 3.3% when $0 \leq \beta \leq 0.7b$ for both cases of delamination depth. The difference reaches 6.3% when $\beta = b$ for delamination depth $0.25h$ and is slightly lower for delamination depth $0.5h$. Again, this is believed to be due to the increasing element size used in the finite element part of the VFM model. As in section 4.1, SM gives very good agreement with the other methods when the plate vibrates globally, e.g. when $0 \leq \beta \leq 0.4b$ in Figures 7 (a) and (c), but with increasing differences between the predicted natural frequencies for wider delaminations when the panel vibrates locally. As the delamination depth is moved to the mid-thickness (Figures 7 (b) and (d)), the global mode remains dominant for wider delaminations and SM shows better agreement with the other methods.

Figure 8 shows normalised mode shape plots of the lowest natural frequency for two cases from Figure 8 obtained from ABAQUS, VFM and SM. For the mid-thickness delamination in Figure 8 (a), the three methods give almost identical mode shapes. But in Figure 8 (b), where the delamination is closer to the top surface, ABAQUS and VFM show good agreement with a maximum difference of 3% in the magnitude of the out of plane displacement, while SM gives a fictitious through-the-length local mode. These findings are further illustrated by the cross-section mode plots in Figure 9.

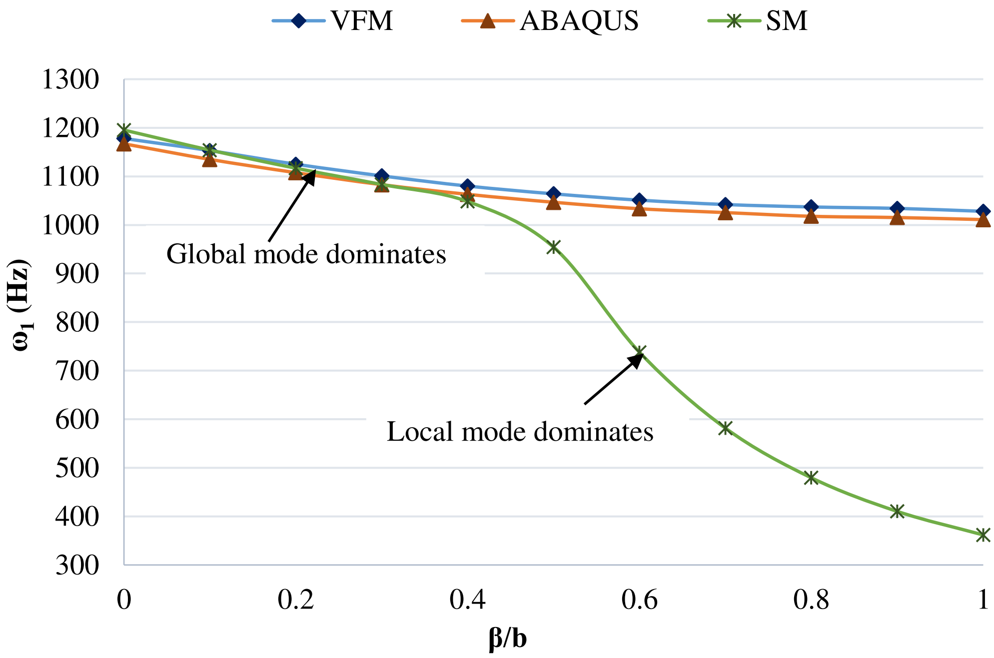

VFM
ABAQUS
SM
1300
1200
1100
1000
900
800
700
600
500
400
300
0
0.2
0.4
0.6
0.8
1
Global mode dominates
Local mode dominates
ω1 (Hz)
β/b

(a)

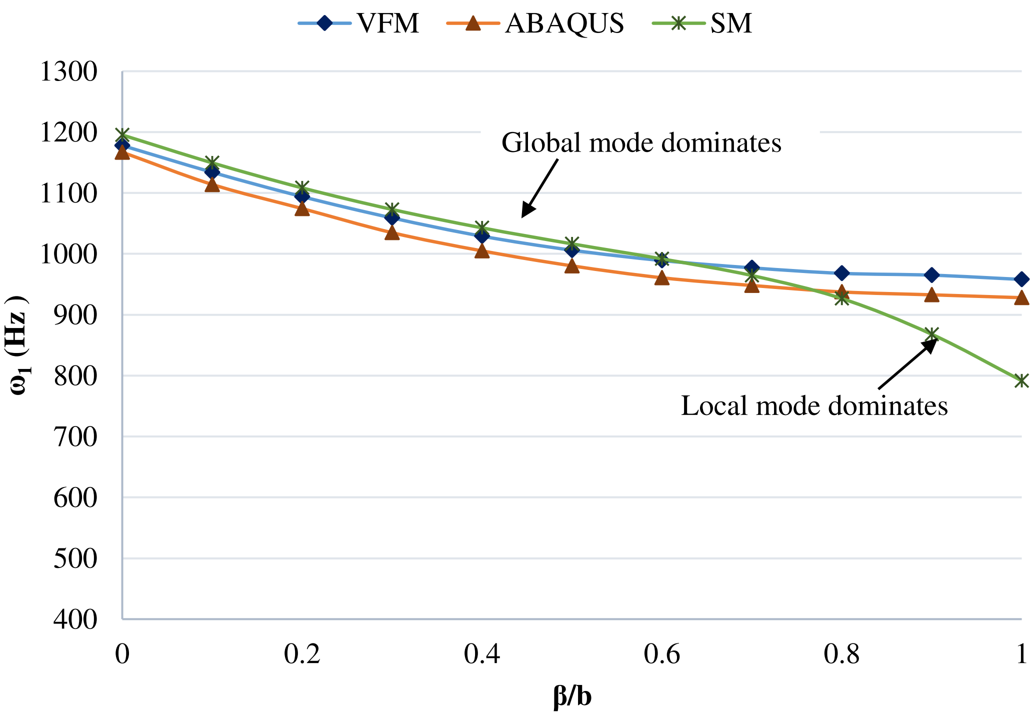

VFM
ABAQUS
SM
1300
1200
1100
1000
900
800
700
600
500
400
0
0.2
0.4
0.6
0.8
1
Global mode dominates
Local mode dominates
ω1 (Hz)
β/b

(b)

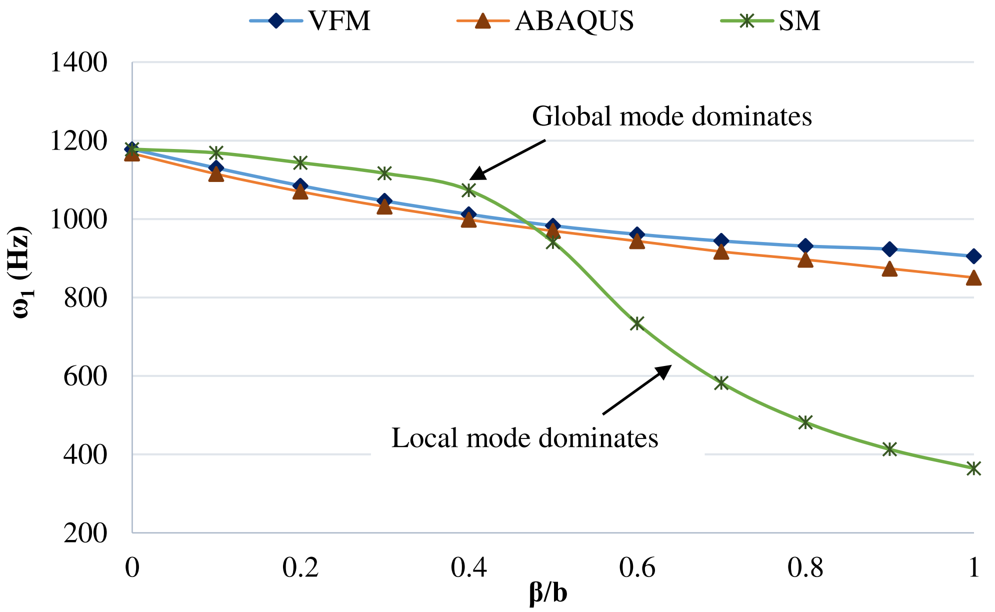

(c)

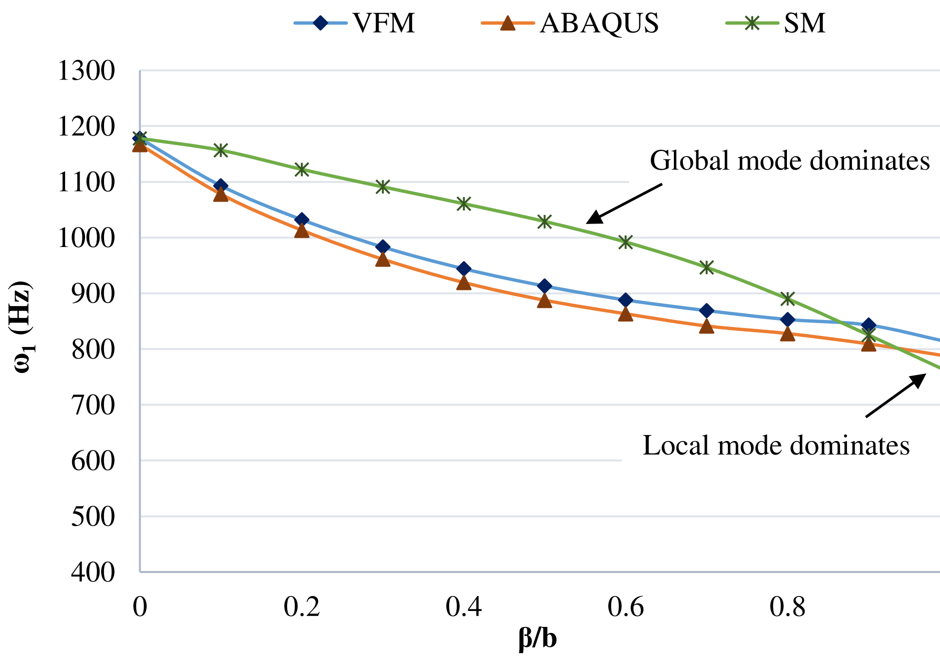

(d)

229 Figure 7. Plots of lowest natural frequency (ω_1) of composite plates against width ratio (β/b) for centrally
230 located embedded rectangular delaminations, using VFM, ABAQUS and SM. (a) Delamination length $d =$
231 $0.25l$, depth $0.25h$. (b) Delamination length $d = 0.25l$, depth $0.5h$. (c) Delamination length $d = 0.5l$,
232 depth $0.25h$. (d) Delamination length $d = 0.5l$, depth $0.5h$.

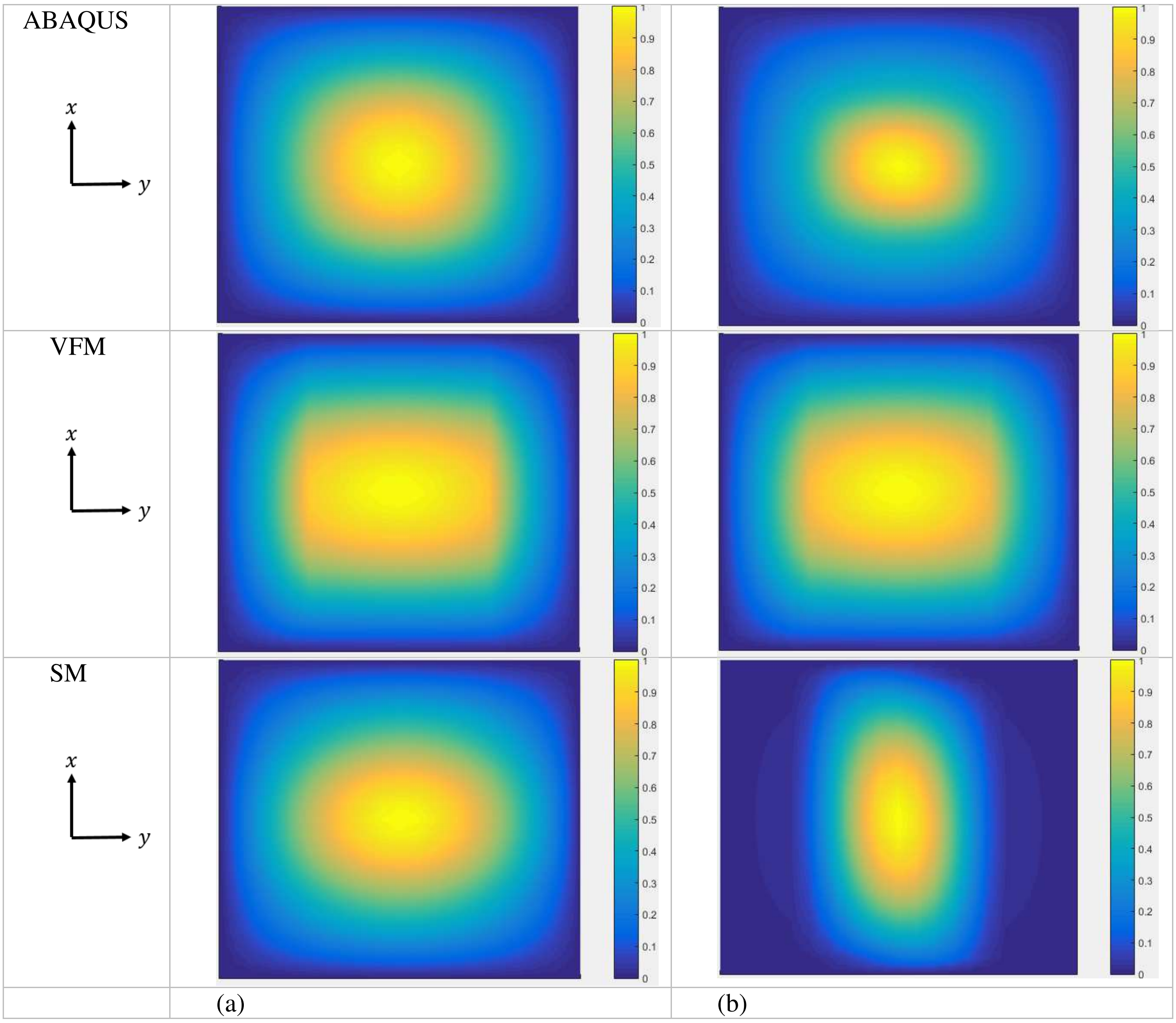

Figure 8. ABAQUS, VFM and SM plots of the normalised mode shape of the lowest natural frequency for a composite plate containing an embedded rectangular delamination. (a) Delamination length $d = 0.5l$, depth $0.5h$, width $\beta = 0.5b$, see Figure 7 (d). (b) Delamination length $d = 0.5l$, depth $0.25h$, width $\beta = 0.6b$, see Figure 7 (c).

4.3 Effect of delamination location

In sections 4.1 and 4.2 VFM was validated for modelling centrally located damage. The effects of lengthwise and widthwise positions (x, y) of the delamination on the lowest natural frequency of a plate will now be studied using VFM and ABAQUS. Figure 10 shows a plate containing embedded delaminations D_1, located at $(a_x, b/2)$, and D_2, located at $\left(l/2, a_y\right)$.

Figure 11 shows the results of this analysis for composite plates containing embedded delaminations with lengths $d = 0.25l$, $0.5l$ and $0.75l$, width $\beta = 0.2b$, at depths $0.25h$ and $0.5h$, plotted against the widthwise location a_y. Figure 12 demonstrates the effect of changing the lengthwise position a_x for delaminations of length $d = 0.25l$ and $0.5l$, width $\beta = 0.2b$ and $0.4b$, at depths $0.25h$ and $0.5h$. All cases clearly show a reduction in the lowest natural frequency as the delamination moves toward the centre of the plate. The analyses demonstrate that VFM can handle any possible location and depth of delamination, for both through-the-length and embedded damage. Excellent agreement is seen between VFM and FEA for all the cases studied. The

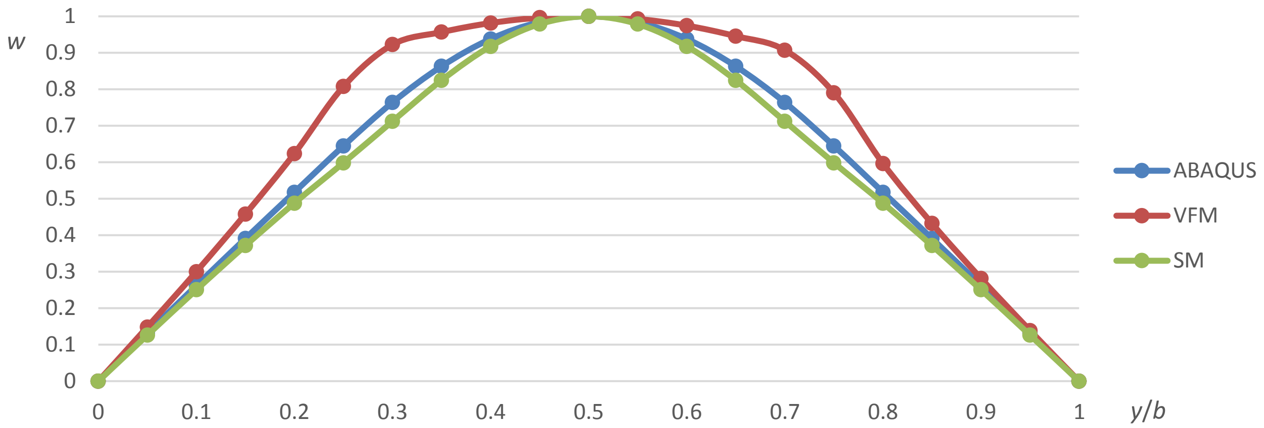

(a)

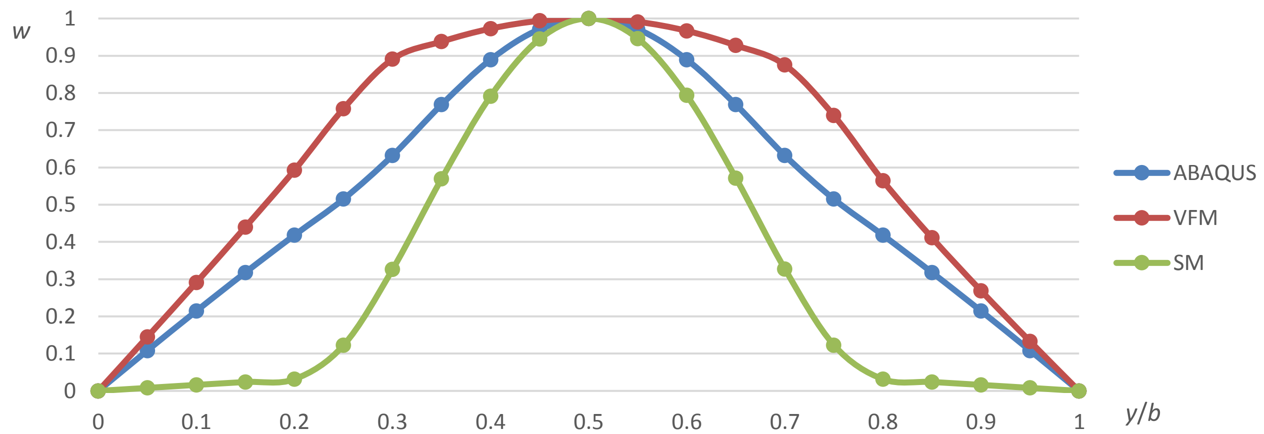

(b)

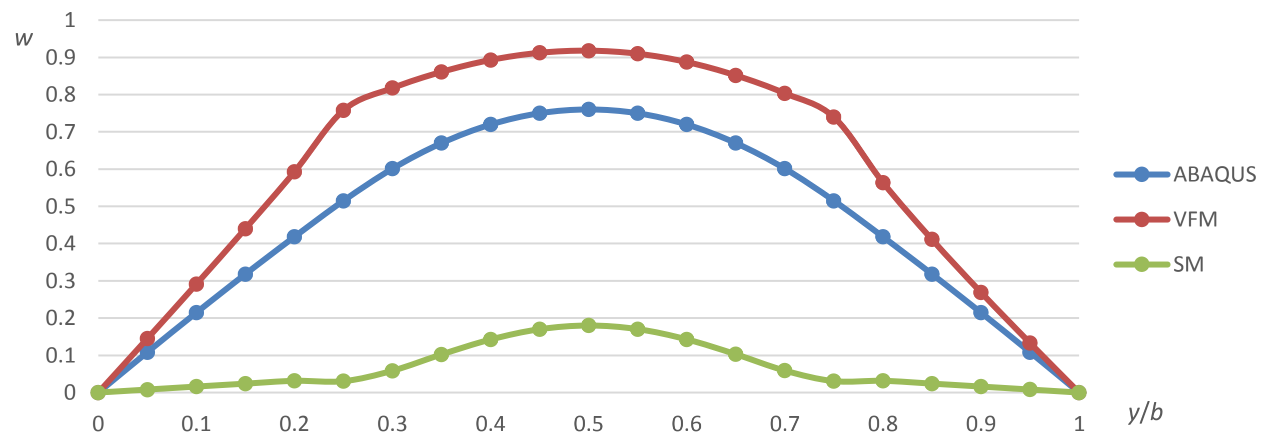

(c)

Figure 9. ABAQUS, VFM and SM cross-section plots of the normalised mode shape of the lowest natural frequency for a composite plate containing an embedded rectangular delamination. (a) Delamination length $d = 0.5l$, depth $0.5h$, width $\beta = 0.5b$, see Figure 7 (d). (b) Top and (c) bottom regions when delamination length $d = 0.5l$, depth $0.25h$, width $\beta = 0.6b$, see Figure 7 (c).

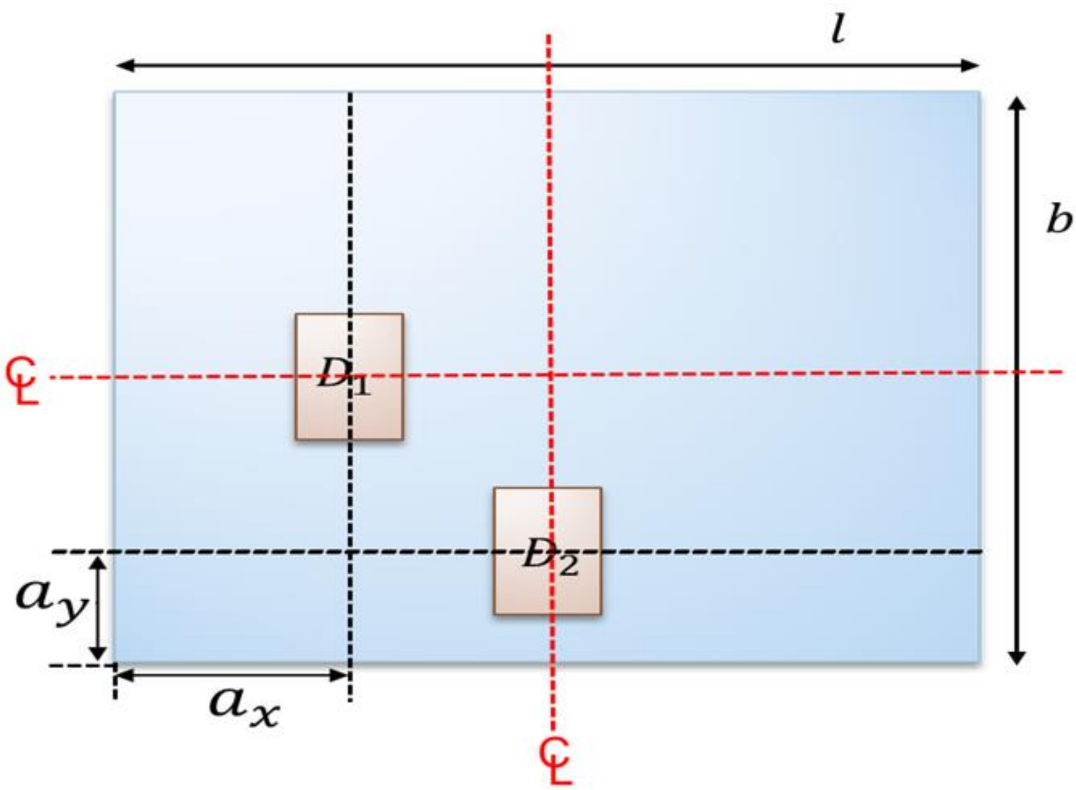

Figure 10. Plate containing arbitrarily located embedded delaminations.

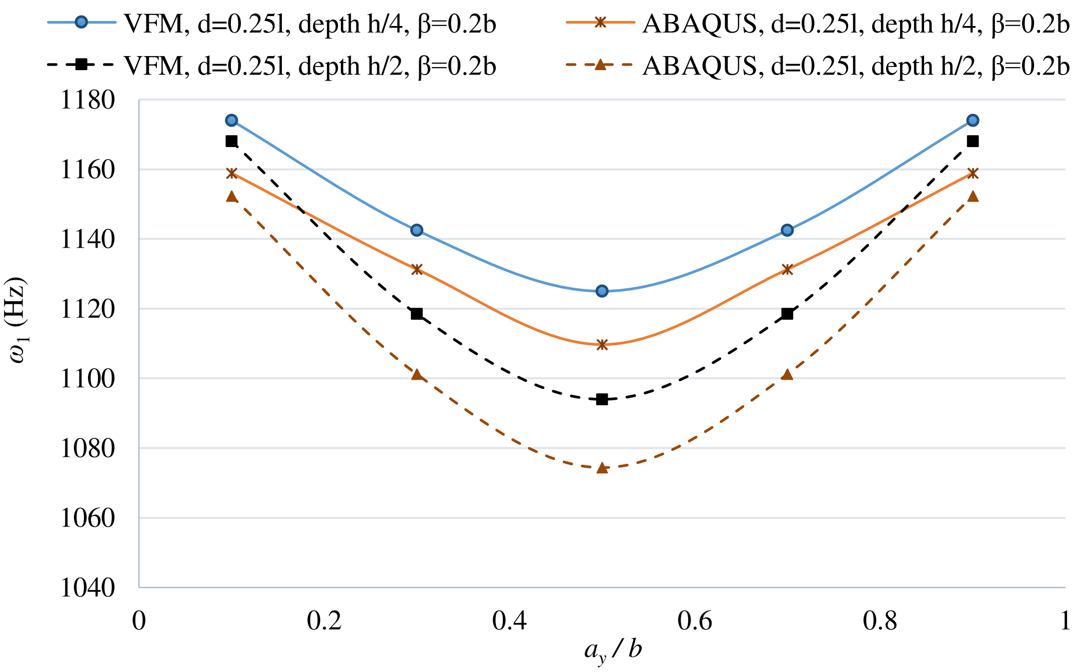

(a)

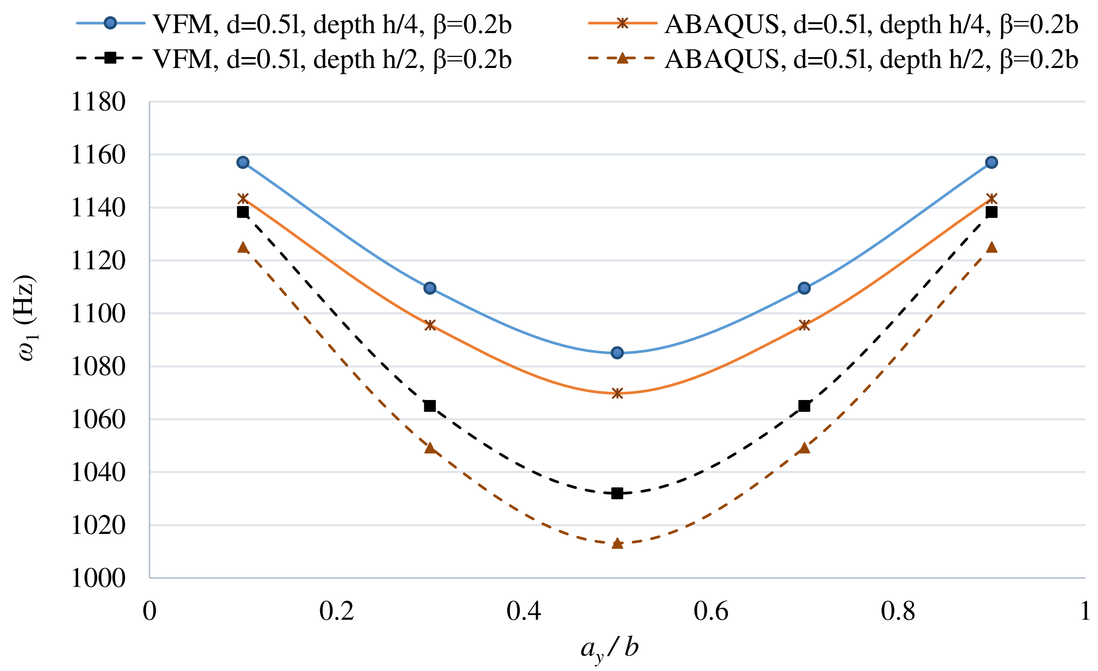

(b)

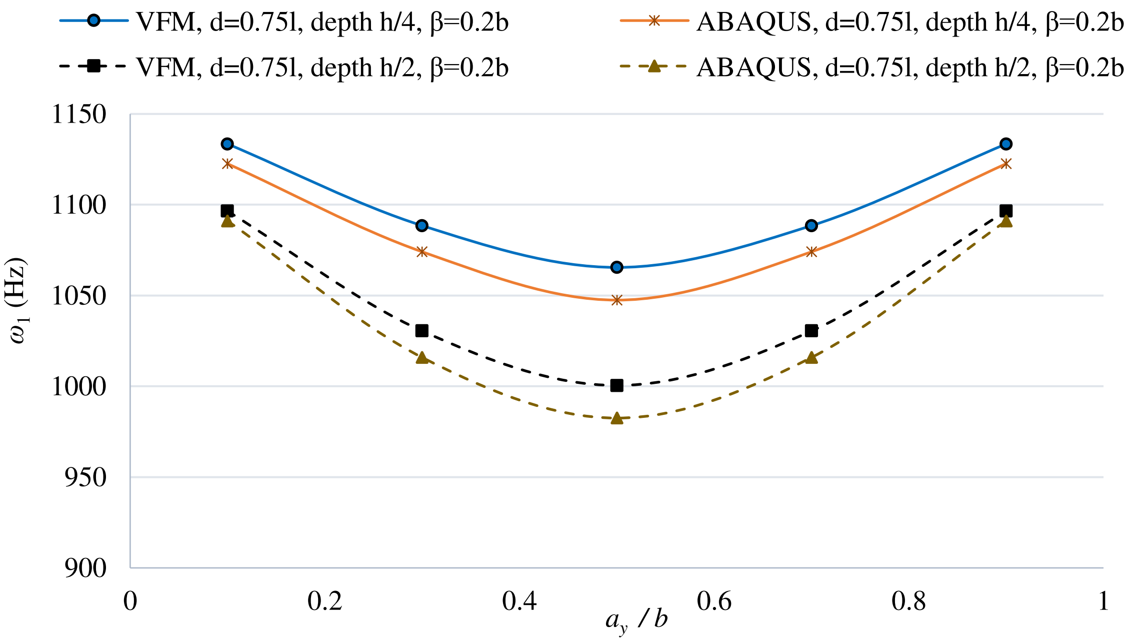

(c)

Figure 11. Plots of the lowest natural frequency (ω_1) of a composite plates against the widthwise position a_y/b of an embedded rectangular delamination.

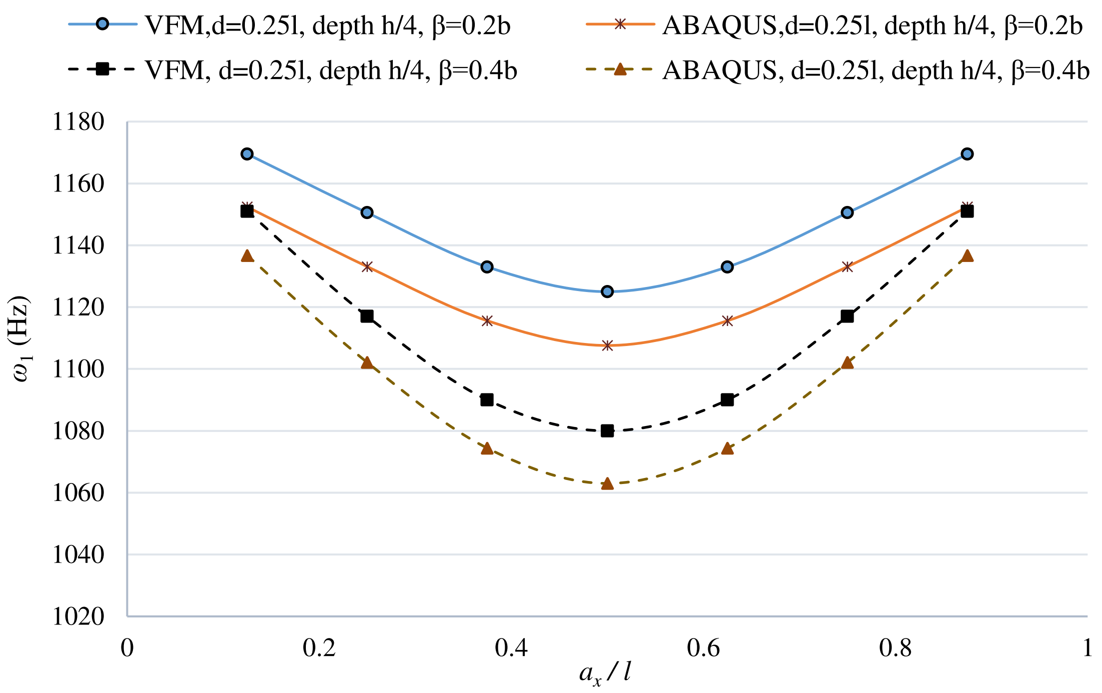

VFM,d=0.25l, depth h/4, β=0.2b
ABAQUS,d=0.25l, depth h/4, β=0.2b
VFM, d=0.25l, depth h/4, β=0.4b
ABAQUS, d=0.25l, depth h/4, β=0.4b
1180
1160
1140
1120
1100
1080
1060
1040
1020
ω1 (Hz)
0
0.2
0.4
0.6
0.8
1
ax / l

(a)

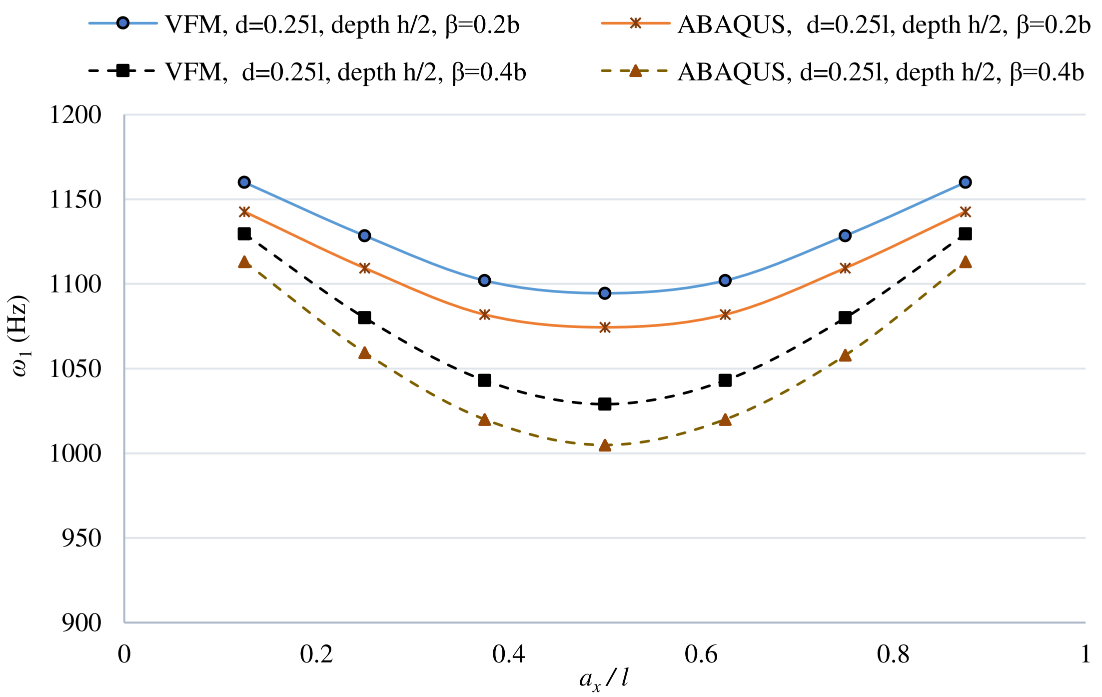

VFM, d=0.25l, depth h/2, β=0.2b
ABAQUS, d=0.25l, depth h/2, β=0.2b
VFM, d=0.25l, depth h/2, β=0.4b
ABAQUS, d=0.25l, depth h/2, β=0.4b
1200
1150
1100
1050
1000
950
900
ω1 (Hz)
0
0.2
0.4
0.6
0.8
1
ax / l

(b)

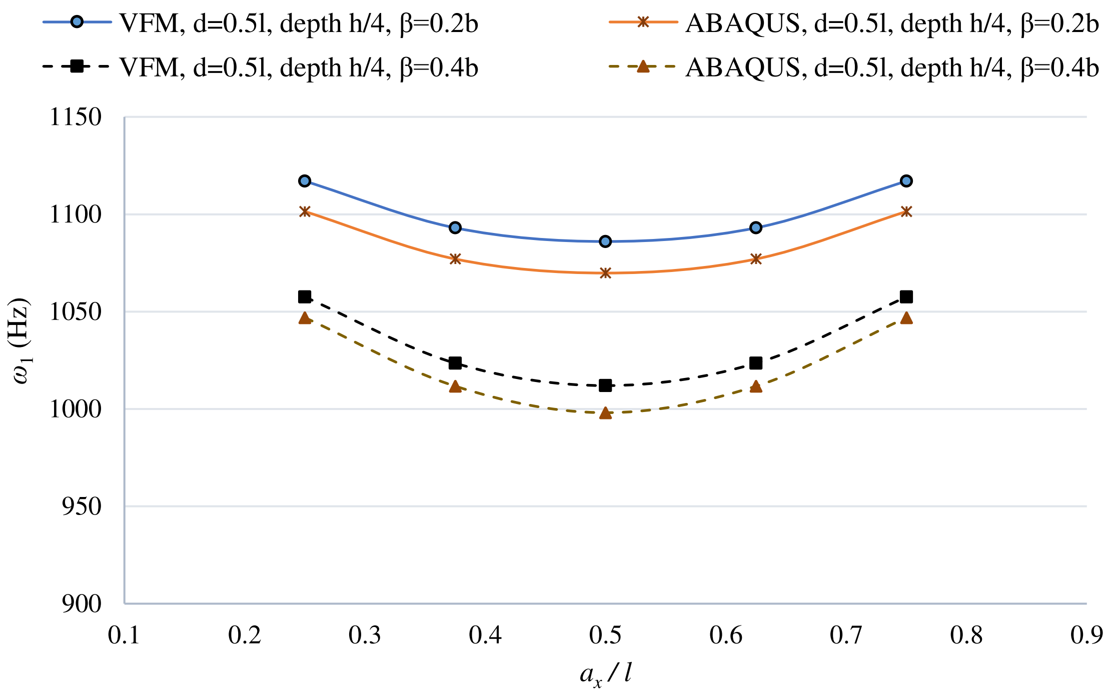

(c)

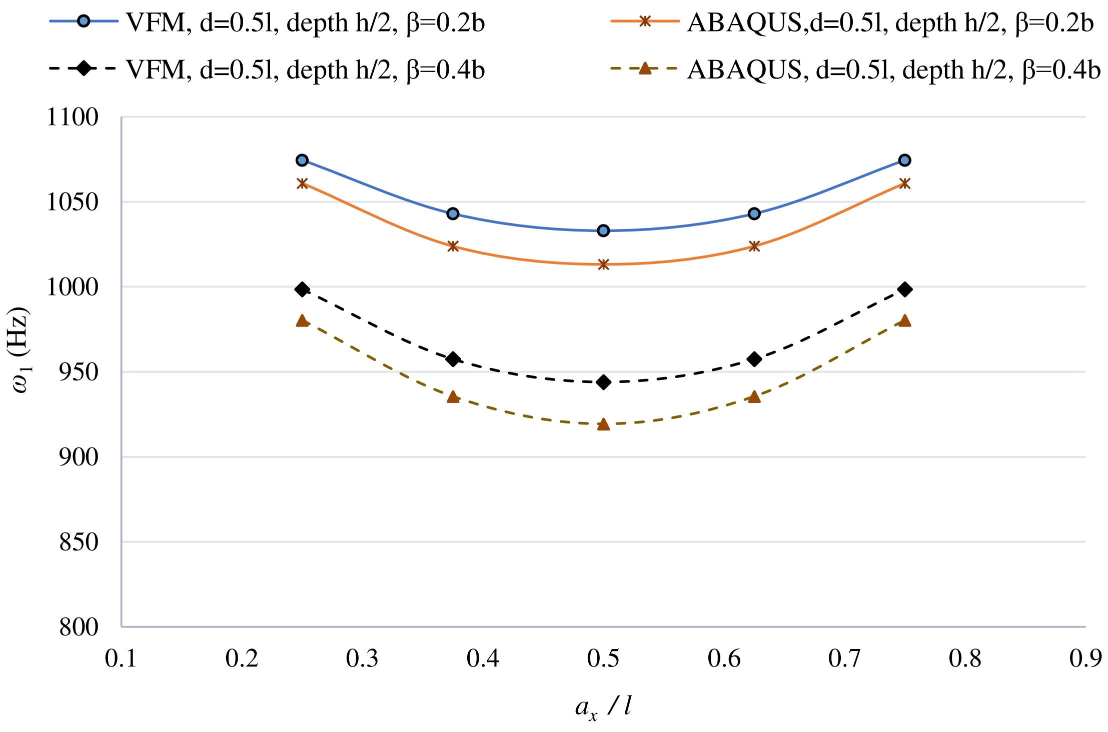

(d)

Figure 12. Plots of lowest natural frequency (ω_1) of a composite plate against the lengthwise position a_x/l of an embedded rectangular delamination.

maximum difference between VFM and FEA was 2.67% for a centrally located delamination with $d = 0.5l$, $\beta = 0.4b$ and depth $0.5h$.

4.4 Effect of aspect ratio on plate containing embedded delamination

Figure 13 illustrates the effect of changing the delamination size for plates with different aspect ratios $\boldsymbol{b/l}$, while Figure 14 shows the reductions in the lowest natural frequency against the aspect ratio. The frequencies are normalized with respect to those of the undamaged plate ($\boldsymbol{\beta/b = 0}$). The maximum difference between VFM and ABAQUS results is just 2.84%. The figures show decreased natural frequencies with increased delamination size and with larger aspect ratios. The degradations in natural frequency tend to be smaller for square plates.

5 Solution time

Anderson et al [16] demonstrated the computational efficiency of the VICON analysis. Williams and Anderson [24] demonstrated additional computational savings for point symmetric structures and for laterally periodic cross-sections. Kennedy et al. [25] again detailed the computational efficiency of exact strip analysis, comparing the program VICONOPT [26] with the FEA program STAGS. Numerical examples, including a composite blade stiffened panel and a ring-stiffened laminated cylinder, confirmed that for comparably converged solutions, VICONOPT was typically between 10^2 and 10^4 times faster than FEA.

For damaged structures, exact strip analysis can only be used when the damage is through-the-length. When modelling embedded damage, Damghani et al. [17] compared the computational efficiency of SM against FEA. A similar assessment will now be made for VFM.

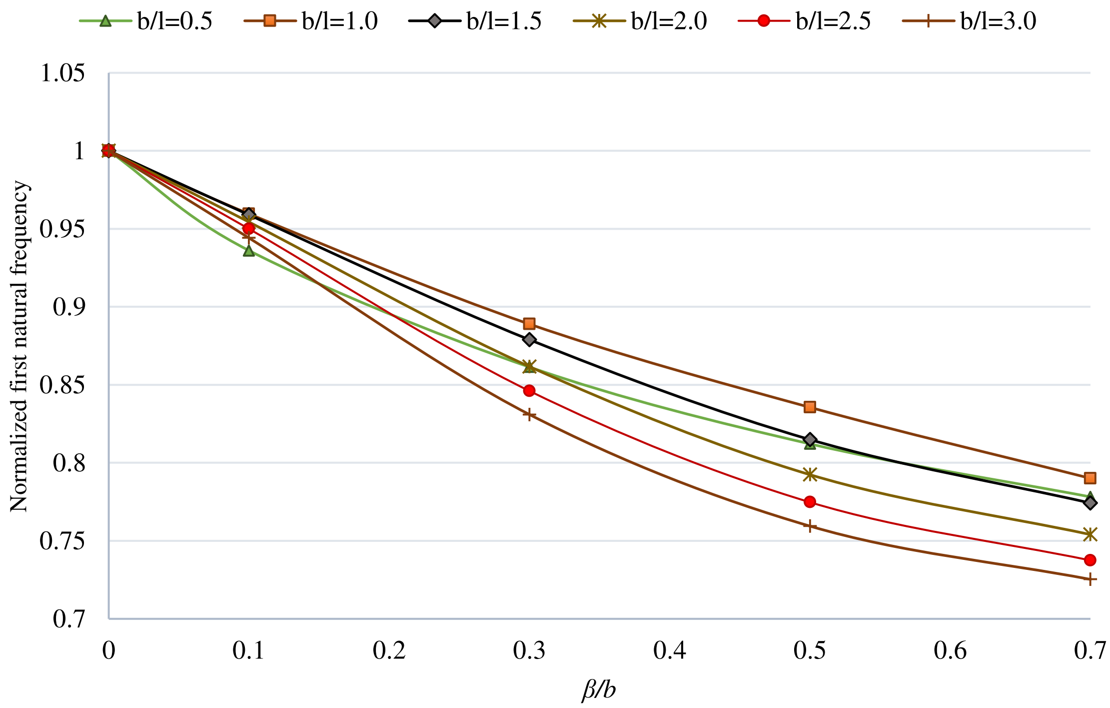

Figure 13. The effect of delamination width β on the lowest natural frequency for a plate with a centrally located delamination of length $d = 0.5l$, having different aspect ratios (b/l).

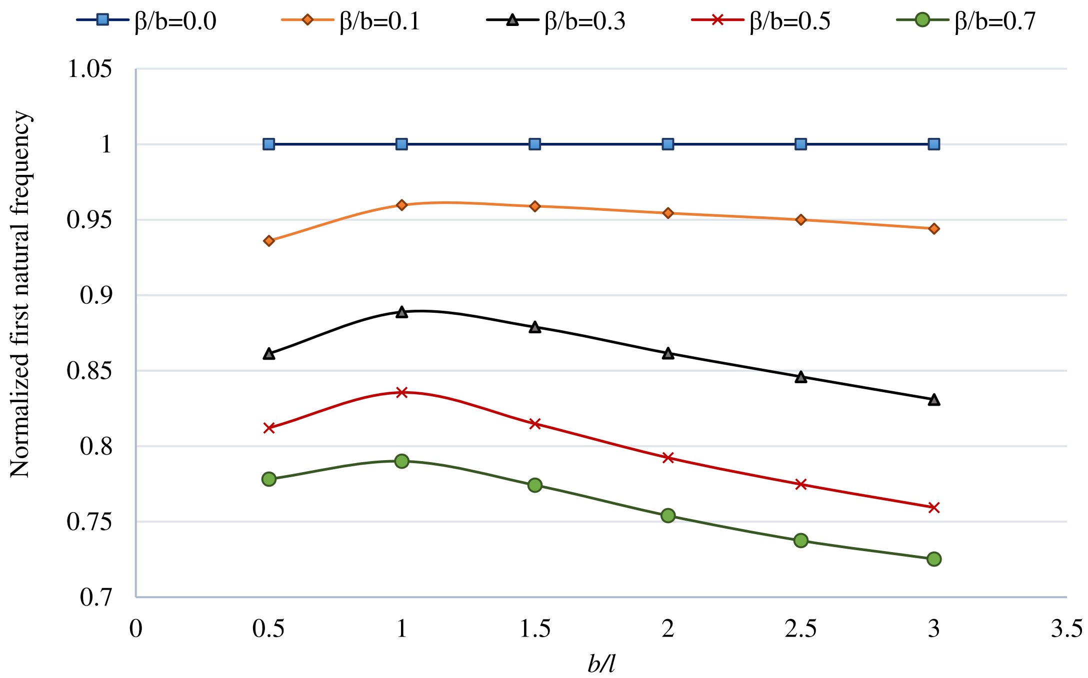

Figure 14. Plots of normalized first natural frequency against aspect ratio (b/l) for a plate with a centrally located delamination of length $d = 0.5l$ and different widths β.

Based on the computational time requirements previously established for VICON analysis [24, 25] and considering only out-of-plane behaviour, the solution time required for one iteration of the Wittrick-Williams algorithm is proportional to

$$W_L = \frac{1}{2}C'\mu N\left(B^2 \times 2^3 + Br \times 2^2 + \frac{4}{3}r^2\right) + \frac{1}{2}CN_{FE}\left(B_{FE}^2 + B_{FE}r + \frac{1}{3}r^2\right) + \frac{1}{6}Cr^3 \qquad (10)$$

C and C' are time constants for real and complex arithmetic respectively, μ is the number of VIPASA matrices used in Eq. (4) and r is the number of constraints applied. The nodes are assumed to be numbered to minimise the bandwidth of the VIPASA and FEA matrices [24]. N and B are the order and bandwidth of each VIPASA matrix, while N_{FE} and B_{FE} are the order and bandwidth of the FEA matrix.

5.1 Application to VFM

Figure 15 (a) shows a plate modelled using VFM. The central portion of the plate is modelled using a finite element mesh of 32 elements (4 × 8). The edge portions are modelled using the exact strip method. The form of the global dynamic stiffness matrix is shown in Figure 15 (b). Applying Eq. (10) shows that the VFM and pure FEA analysis times are, respectively, 7.02 and 29.85 times longer than that of the pure VICON analysis. Thus for through-the-length damage there is a clear computational advantage in using VICON analysis over FEA. In the case of embedded damage, for which pure VICON analysis cannot be used, VFM provides an accurate alternative to pure FEA and is about 4 times faster.

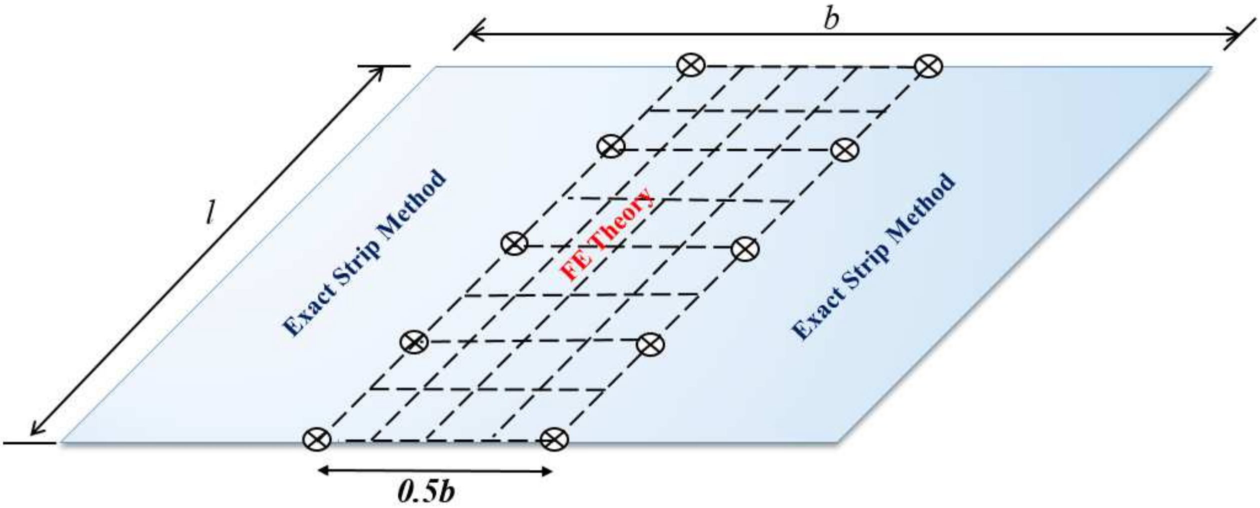

(a)

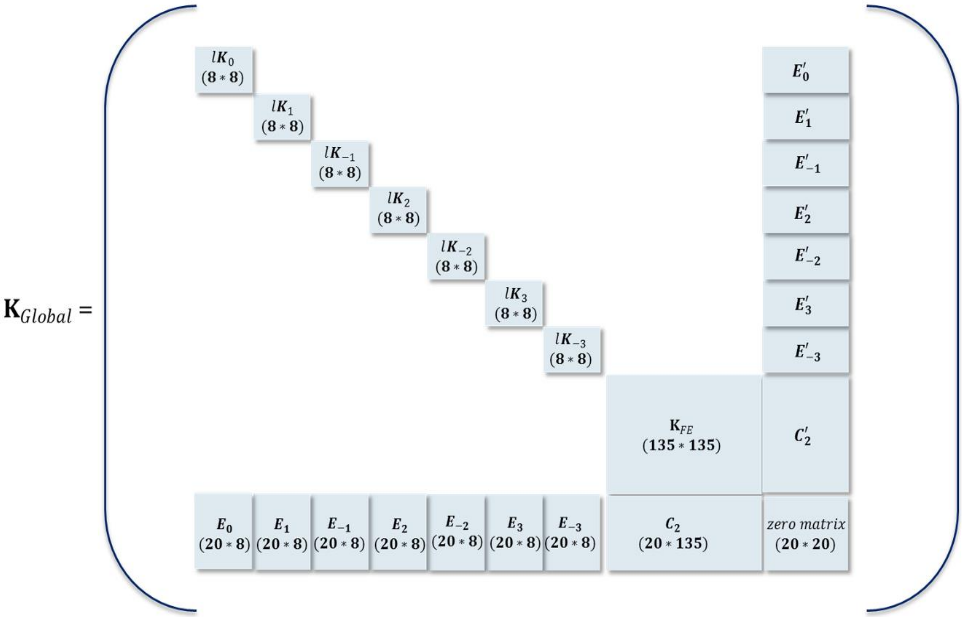

(b)

Figure 15. (a) Damaged plate modelled in VFM. (b) Form of the global dynamic stiffness matrix.

6 Conclusions

A novel technique (VFM) combining the exact strip method with finite element theory (VFM) has been developed to enable the modelling of more complex geometries of damage than the previous smearing method whilst retaining a computational advantage over finite element analysis. To prove the effectiveness of this method, isotropic and composite plates containing through the length and embedded rectangular damage, including delamination, have been examined. VFM has been shown to efficiently handle geometries of damage that the previous exact strip models could not handle. It also shows better agreement with finite element analysis than a previous smearing method which, whilst giving accurate and efficient results for cases of damage where the plates vibrate globally, gives conservative results when the plate undergoes local vibration.

Acknowledgements

This work was supported by the Libyan Ministry of Higher Education.

References

[1] S. Y. Lee and D. Y. Park, "Buckling analysis of laminated composite plates containing delaminations using the enhanced assumed strain solid element," *International Journal of Solids and Structures,* vol. 44, pp. 8006-8027, 2007.

[2] Y. Pekbey and O. Sayman, "A numerical and experimental investigation of critical buckling load of rectangular laminated composite plates with strip delamination," *Journal of Reinforced Plastics and Composites,* vol. 25, pp. 685-697, 2006.

[3] F. Cappello and D. Tumino, "Numerical analysis of composite plates with multiple delaminations subjected to uniaxial buckling load," *Composites Science and Technology,* vol. 66, pp. 264-272, 2006.

[4] B. L. Karihaloo and H. Stang, "Buckling-driven delamination growth in composite laminates: Guidelines for assessing the threat posed by interlaminar matrix delamination," *Composites Part B: Engineering,* vol. 39, pp. 386-395, 2008.

[5] P. F. Liu, S. J. Hou, J. K. Chu, X. Y. Hu, C. L. Zhou, Y. L. Liu*, et al.*, "Finite element analysis of postbuckling and delamination of composite laminates using virtual crack closure technique," *Composite Structures,* vol. 93, pp. 1549-1560, 2011.

[6] S. F. Nikrad, S. Keypoursangsari, H. Asadi, A. H. Akbarzadeh, and Z. T. Chen, "Computational study on compressive instability of composite plates with off-center delaminations," *Computer Methods in Applied Mechanics and Engineering,* vol. 310, pp. 429-459, 2016.

[7] S. Yazdani, W. J. H. Rust, and P. Wriggers, "Delamination growth in composite laminates of variable stiffness," *International Journal for Numerical Methods in Engineering,* vol. 108, pp. 1406-1424, 2016.

[8] A. Szekrényes, "Application of Reddy's third-order theory to delaminated orthotropic composite plates," *European Journal of Mechanics, A / Solids,* vol. 43, pp. 9-24, 2014.

[9] T. Park, S. Y. Lee, and G. Z. Voyiadjis, "Finite element vibration analysis of composite skew laminates containing delaminations around quadrilateral cutouts," *Composites Part B: Engineering,* vol. 40, pp. 225-236, 2009.

[10] S. Devendiran, K. Manivannan, K. Venkatesan, A. T. Mathew, A. Thakur, and V. Ashish Chauhan, "Free vibration of damaged and undamaged hybrid CFRP/GFRP composite laminates," *International Journal of Mechanical Engineering and Technology,* vol. 8, pp. 349-360, 2017.

[11] Z.-X. Wang, P. Qiao, and J. Xu, "Vibration analysis of laminated composite plates with damage using the perturbation method," *Composites Part B: Engineering,* vol. 72, pp. 160-174, 2015.

[12] I. N. Jayatilake, W. Karunasena, and W. Lokuge, "Finite element based dynamic analysis of multilayer fibre composite sandwich plates with interlayer delaminations," *Advances in Aircraft and Spacecraft Science,* vol. 3, pp. 15-28, 2016.

[13] X. W. Wang, I. Pont-Lezica, J. M. Harris, F. J. Guild, and M. J. Pavier, "Compressive failure of composite laminates containing multiple delaminations," *Composites Science and Technology,* vol. 65, pp. 191-200, 2005.

[14] D. Kennedy, M. Fischer, and C. A. Featherson, "Recent developments in exact strip analysis and optimum design of aerospace structures," *Proceedings of the Institution of Mechanical Engineers, Part C: Journal of Mechanical Engineering Science,* vol. 221, pp. 399-413, 2007.

[15] R. Butler, A. T. Rhead, W. Liu and N. Kontis, "Compressive strength of delaminated aerospace composites", *Philosophical Transactions of The Royal Society A*, vol. 370, pp. 1759-1779, 2012.

[16] M. S. Anderson, F. W. Williams, and C. J. Wright, "Buckling and vibration of any prismatic assembly of shear and compression loaded anisotropic plates with an arbitrary supporting structure," *International Journal of Mechanical Sciences,* vol. 25, pp. 585-596, 1983.

[17] M. Damghani, D. Kennedy, and C. Featherston, "Global buckling of composite plates containing rectangular delaminations using exact stiffness analysis and smearing method," *Computers and Structures,* vol. 134, pp. 32-47, 2014.

[18] M. Damghani, D. Kennedy, and C. Featherston, "Critical buckling of delaminated composite plates using exact stiffness analysis," *Computers and Structures,* vol. 89, pp. 1286-1294, 2011.

[19] W. H. Wittrick and F. W. Williams, "A general algorithm for computing natural frequencies of elastic structures," *Quarterly Journal of Mechanics and Applied Mathematics,* vol. 24, pp. 263-284, 1971.
[20] W. H. Wittrick and F. W. Williams, "Buckling and vibration of anisotropic or isotropic plate assemblies under combined loadings," *International Journal of Mechanical Sciences,* vol. 16, pp. 209-239, 1974.
[21] F. W. Williams and M. S. Anderson, "Incorporation of Lagrangian Multipliers into an algorithm for finding exact natural frequencies or critical buckling loads," *International Journal of Mechanical Sciences,* vol. 25, pp. 579-584, 1983.
[22] DS Simulia Inc. ABAQUS Standard Manual (version 6.10). 2012.
[23] J. S. Przemieniecki, *Theory of Matrix Structural Analysis*: Dover, 1985.
[24] F. W. Williams and M. S. Anderson, "Buckling and vibration analysis of shear-loaded prismatic plate assemblies with supporting structures, utilizing symmetric or repetitive cross-sections. In: *Aspects of the Analysis of Plate Structures - A Volume in Honour of W.H. Wittrick* (ed. D. J. Dawe, R. W. Horsington, A. G. Kamtekar and G. H. Little), Oxford, 1985, pp. 51-71.
[25] D. Kennedy, F. W. Williams, and M. S. Anderson, "Buckling and vibration analysis of laminated panels using viconopt," *Journal of Aerospace Engineering,* vol. 7, pp. 245-262, 1994.
[26] F. W. Williams, D. Kennedy, M. S. Anderson, and R. Butler, "VICONOPT - Program for exact vibration and buckling analysis or design of prismatic plate assemblies," *AIAA Journal,* vol. 29, pp. 1927-1928, 1991.